

Early Archaean hydrothermal fluids; a study of inclusions from the ~3.4 Ga Buck Ridge Chert, Barberton Greenstone Belt, South Africa

Sjoukje T. de Vries^{a,*}, Jacques L.R. Touret^{b,1}

^a Department of Earth Sciences, Utrecht University, Budapestlaan 4, 3584 CD Utrecht, The Netherlands

^b Faculty of Earth and Life Sciences, Free University of Amsterdam, De Boelelaan 1085, 1081 HV Amsterdam, The Netherlands

Accepted 30 June 2006

Editor: R.L. Rudnick

Abstract

Fluid inclusions have been studied from cavities and breccias in one of the oldest well-preserved, relatively low-grade metamorphosed sedimentary sequences on Earth. The fluid inclusion-bearing samples are from the uppermost part of the early Archaean (~3.4 Ga) Buck Ridge volcano-sedimentary complex in the Barberton Greenstone Belt (South Africa), which was affected by hydrothermal alteration during and immediately after its deposition. In banded, silicified sandy sediments this alteration is characterised, among other features, by quartz-cemented hydrothermal breccias, layer-bound stockworks of cm-size quartz veins and quartz-filled cavities below stacked pebbles. Quartz grains in these hydrothermal deposits contain numerous fluid inclusions filled with either two-phase aqueous or mixed H₂O–CO₂ fluid. The aqueous inclusions are divided into three different groups, based on their microthermometric characteristics: type H_A (relatively high salinity), type M_A (intermediate salinity) and type L_A (relatively low salinity). Optical and microthermometric characteristics of the fourth type of inclusions, the mixed H₂O–CO₂ fluid (type C) indicate that it was homogeneous at the time of trapping, with only some minor changes occurring after trapping.

Type H_A and type C fluids appear as immiscible fluids in their host crystal, most probably resulting from unmixing of the hydrothermal fluid. Phase relations in the CO₂–H₂O system show that the unmixing must have occurred at a relatively low pressure of ~100 bars. This conclusion is in line with the geological context of the samples, which indicates a shallow environment of deposition for the sediments, (almost) contemporaneous hydrothermal activity, and a very low metamorphic grade. However, it is contrary to the first impression given by the homogeneous character of type C inclusions, which suggests much higher *P–T* conditions at the time of trapping. The aqueous component of type C fluids may have progressively mixed with high-salinity aqueous fluids (type H_A), resulting in a dilution trend from H_A to M_A to L_A fluids. The hydrothermal fluids from the Buck Ridge Chert in the Barberton Greenstone Belt are strikingly similar to those encountered in present-day systems. They show minor differences with older (ca. 3.8 Ga) fluids preserved in hydrothermally altered rocks from the Isua Greenstone Belt in Greenland.

© 2006 Elsevier B.V. All rights reserved.

Keywords: Fluid inclusions; Hydrothermal system; Barberton Greenstone Belt; Buck Ridge volcano-sedimentary complex; Hooggenoeg Formation; Onverwacht Group

1. Introduction

The study of fluid inclusions is an important tool in geology, because the inclusions potentially contain direct remnants of the fluids that once circulated through

* Corresponding author. Tel.: +61 2 6283 4800.

E-mail address: stdevries@geo.uu.nl (S.T. de Vries).

¹ Present address: Musée de Minéralogie, Ecole des Mines, 60 Bvd Saint Michel, 75006 Paris, France.

the rock pile. Studying inclusions from early Archaean rocks is especially interesting, since knowledge about the hydrosphere at that time is extremely limited. Fluid inclusion studies have been performed on Archaean (>2.5 Ga) rocks, but mainly on hydrothermal ore deposits (mostly gold). Fluid inclusion data on other Archaean magmatic and metamorphic fluids are limited (for an overview see De Ronde et al., 1997b). Studies on fluid inclusions in *early* (~3.8–3.3 Ga) to *mid* (~3.3–3.0 Ga) Archaean rocks are scarce (e.g. De Ronde et al., 1994, 1997a; Kitajima et al., 2001a,b; Appel et al., 2001; Touret, 2003), especially those related to fluids at or near the Earth's surface.

In this article, fluid inclusion data from cavities and breccias in early Archaean (~3.4 Ga old) *sedimentary* rocks of the Buck Ridge volcano-sedimentary complex (BR-vsc) in the Barberton Greenstone Belt (South Africa, Fig. 1) are presented. The BR-vsc forms the uppermost part of the Hoogenoeg Formation and has a well-known geological setting (Fig. 1 and below). The sediments at the top of the BR-vsc were affected by hydrothermal activity during and shortly after deposi-

tion (De Vries, 2004). Hydraulic breccia bodies and quartz-filled cavities in the sediments were related to, or formed as a result of this hydrothermal activity. Fluid inclusions in these deposits may therefore provide information about the temperature, pressure and composition of the fluids that once circulated through this ~3.4 Ga old hydrothermal system.

2. Location and description of the investigated samples

2.1. Geological setting

The Barberton Greenstone Belt (South Africa) contains some of the best-preserved early Archaean sedimentary rocks on Earth. The Onverwacht Group, the oldest group in this greenstone belt, comprises predominantly mafic and ultramafic rocks, with minor intercalations of chertified sediments (e.g. De Wit and Ashwal, 1997; Lowe and Byerly, 1999). The uppermost part of the Onverwacht Group is formed by the ~3.45–3.16 Ga Buck Ridge volcano-sedimentary complex (BR-vsc, Fig. 1), which consists of

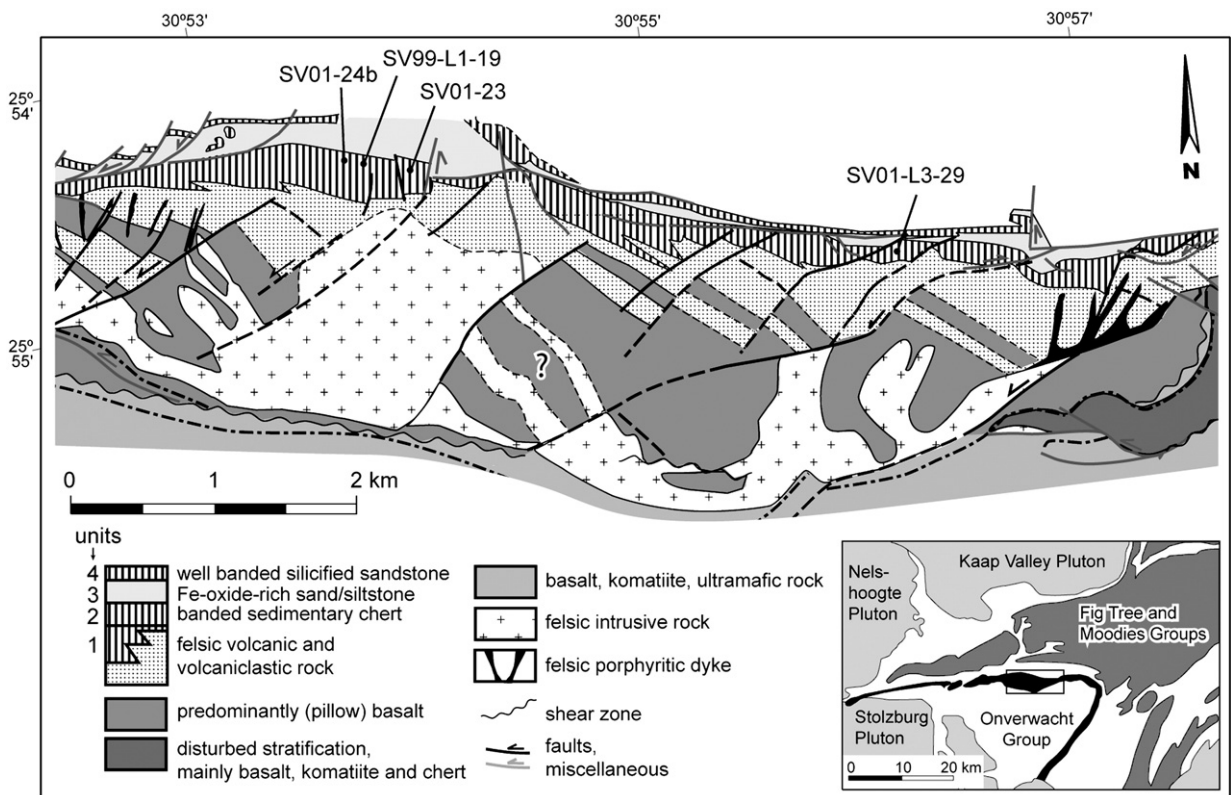


Fig. 1. Geological map of part of the Buck Ridge volcano-sedimentary complex, for location in southern Barberton Greenstone Belt see inset. Simplified after De Vries et al. (2006). All four samples are from unit 2, a banded sedimentary chert that forms part of the silicified sedimentary sequence in the uppermost part of the BR-vsc. Sample locations are indicated. Legend applies to main figure only, not to inset.

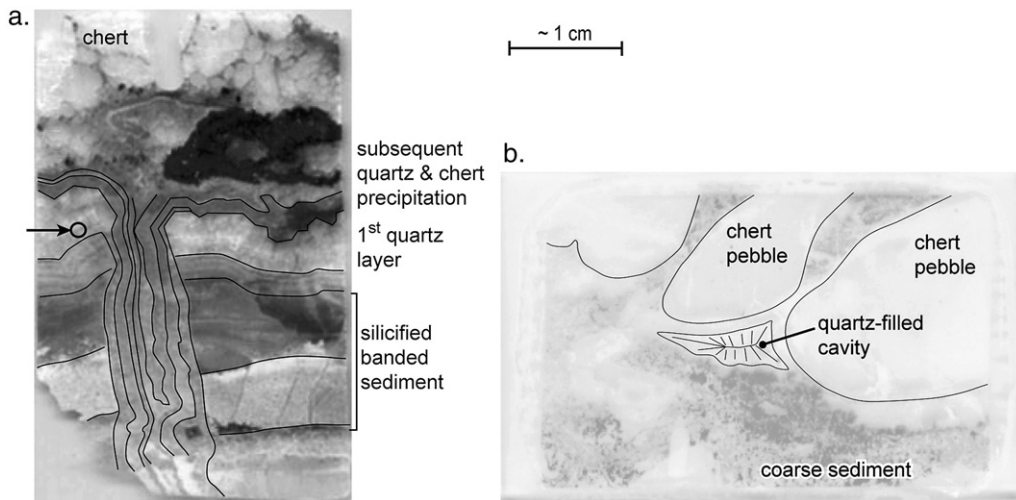


Fig. 2. a. Sample SV99-L1-19; analysed inclusions are from a grain within the circle. b. Sample SV01-L3-29; analysed fluid inclusions are from quartz-filled cavity below chert pebbles.

an alternation of basalts with felsic lavas and felsic porphyries, and a capping silicified sedimentary sequence. The rocks in the study area only experienced very low-grade metamorphism (e.g. Kisch and Nijman, 2004). The sedimentary top of the BR-vsc, the Buck Ridge Chert (BRC), consists from old to young of four units: (1) a partly silicified volcanoclastic unit, (2) a banded sedimentary chert, (3) an iron-oxide-rich sandstone–siltstone interval with dispersed breccia bodies and, (4) a well-banded silicified sandstone. Deposition of the BR-vsc took place during activity of large-scale normal faults (De Vries et al., 2006). The sediments were subject to heavy alteration and became silicified during and/or soon after deposition. For details on the sedimentary and diagenetic environment of the BRC, see De Vries (2004) and De Vries et al. (in preparation).

Contemporaneous with faulting and BR-vsc deposition, a hydrothermal system was active. Preserved remnants of this system include metre-wide black chert veins that cut through the felsic volcanic rocks, and numerous types of veins and breccias in the overlying capping sedimentary sequence.

2.2. Investigated samples

Four samples from BR-vsc unit 2 (i.e. the banded sedimentary chert) were selected for the fluid inclusion study; three from the central part of the study area (SV99-L1-19, SV01-23 and SV01-24b) and one from the same unit further to the east (SV01-L3-29, for locations see Fig. 1).

Inclusions in samples SV99-L1-19 and SV01-23 are hosted by quartz veins. Sample SV99-L1-19 shows both bedding-parallel and bedding-perpendicular quartz and chert cutting through a multi-coloured banded chert (Fig. 2a). Bedding-parallel layers of quartz crystals are interpreted to have formed first, and were subsequently coated by multiple layers of precipitated quartz and chert. Primary inclusions hosted by the bedding-parallel quartz are therefore expected to represent the earliest fluids in the system. In sample SV01-23, a quartz vein cuts step-wise through grey, banded, sandy sediments. It forms part of a layer-bound stockwork of veins that are cut by small-scale faults. Time control on the growth of quartz in this sample is limited.

Inclusions in sample SV01-24b are hosted by quartz that forms the cement to a breccia in BR-vsc unit 2. The breccia body is discordant with bedding and is associated with intense (local) veining of BRC unit 2. The breccia was generated *in situ*; fragments of host rock rotated and moved slightly with respect to each other. The small displacement of adjacent blocks suggests limited fluid overpressure during the breccia formation. The breccia is interpreted to have formed as a result of hydraulic fracturing and fluid flow at very shallow depth, just below the surface.

The fourth sample (SV01-L3-29) was taken about 4 km along strike to the east. The studied inclusions are hosted by quartz that fills a cavity below two chert pebbles (Fig. 2b). The pebbles are interpreted to have been stacked during deposition, leaving voids through which early diagenetic fluids could circulate and in which the quartz could precipitate.

3. Method

A doubly polished, 100 μm thick section was made of each of the four samples. From each section, up to five quartz grains were selected and their fluid inclusions precisely drawn. For microthermometric measurements, an Olympus BH-2 microscope with a Linkam THM600 freezing/heating stage connected to a Linkam CS196 cooling system and a TP91 heating system were used. The stage was calibrated against the melting point of CO_2 in $\text{H}_2\text{O}/\text{CO}_2$ inclusions in quartz from Binn, Switzerland ($T_m = -56.6^\circ\text{C}$). Melting temperatures were recorded at $1^\circ\text{C}/\text{min}$, homogenisation temperatures at $1\text{--}5^\circ\text{C}/\text{min}$. All measurements were repeated at least once. Reproducibility is better than $\pm 0.1^\circ\text{C}$ for the melting temperatures and $\pm 0.5^\circ\text{C}$ for the homogenisation temperatures.

4. Results

4.1. Visual characteristics of the inclusions

Quartz-hosted fluid inclusions from the BR-vsc are generally very small. The average size of the analysed

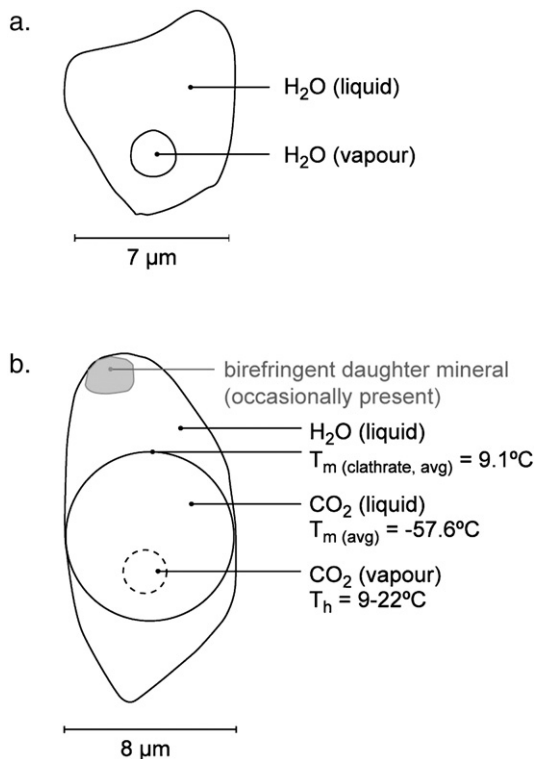


Fig. 3. a. Schematic drawing of a typical aqueous inclusion. For a summary of microthermometric data see Table 1 and Fig. 8. b. Schematic drawing of a typical type C inclusion, with a summary of microthermometric data.

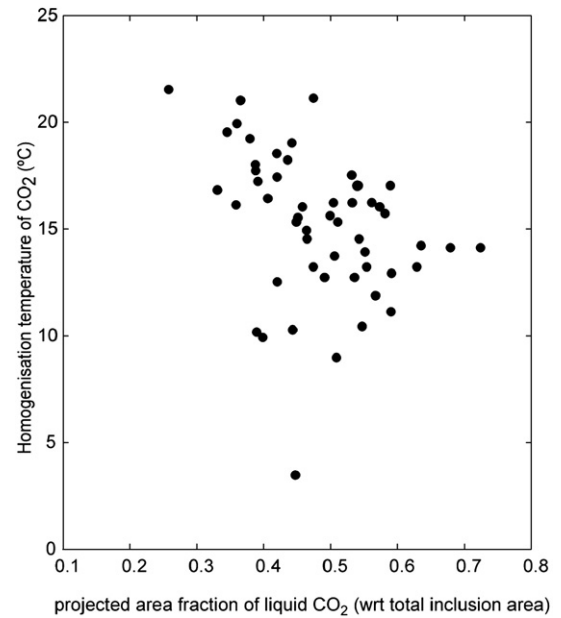


Fig. 4. Homogenisation temperature of CO_2 vs. projected area fraction of the liquid CO_2 for type C inclusions in sample SV01-23. The fraction was calculated using the program Image Tool and digital images of the individual inclusions. The distribution shows that the projected area fraction of liquid CO_2 (and hence also the volume %) is fairly homogeneous, and there are no indications for major post-trapping changes.

inclusions is 7–8 μm , but most of the inclusions are much smaller. Visual inspection did not reveal any obvious differences in characteristics between the analysed inclusions and the smaller inclusions. Based on visual observation, two categories of inclusions were identified. The first category of inclusions contains aqueous liquid+vapour at room temperature (Fig. 3a), and shows a relatively constant volume fraction of vapour. The average vapour content of this category of inclusions, based on comparison charts by Roedder (1984) and Mercolli (1979), is $\ll 10$ vol.%. Inclusions of the second category (type C inclusions) consist of liquid water+liquid CO_2 ±vapour CO_2 at room temperature (Fig. 3b). Occasionally, a birefringent solid, presumably calcite, is also present. At room temperature, the projected area fraction of the liquid CO_2 is relatively constant, roughly between 0.35 and 0.60 (average fraction 0.48; Fig. 4). Based on the rather flat shape of the inclusions, the area fraction is taken to be equal to the volume fraction ($V_{\text{CO}_2}/V_{\text{total}}$; this is probably a slight overestimate of the true volume ratio; cf. Roedder, 1984). There are no petrographic indications of significant post-entrapment changes of type C inclusions, such as partial decrepitation or ‘necking down’ (Roedder, 1984).

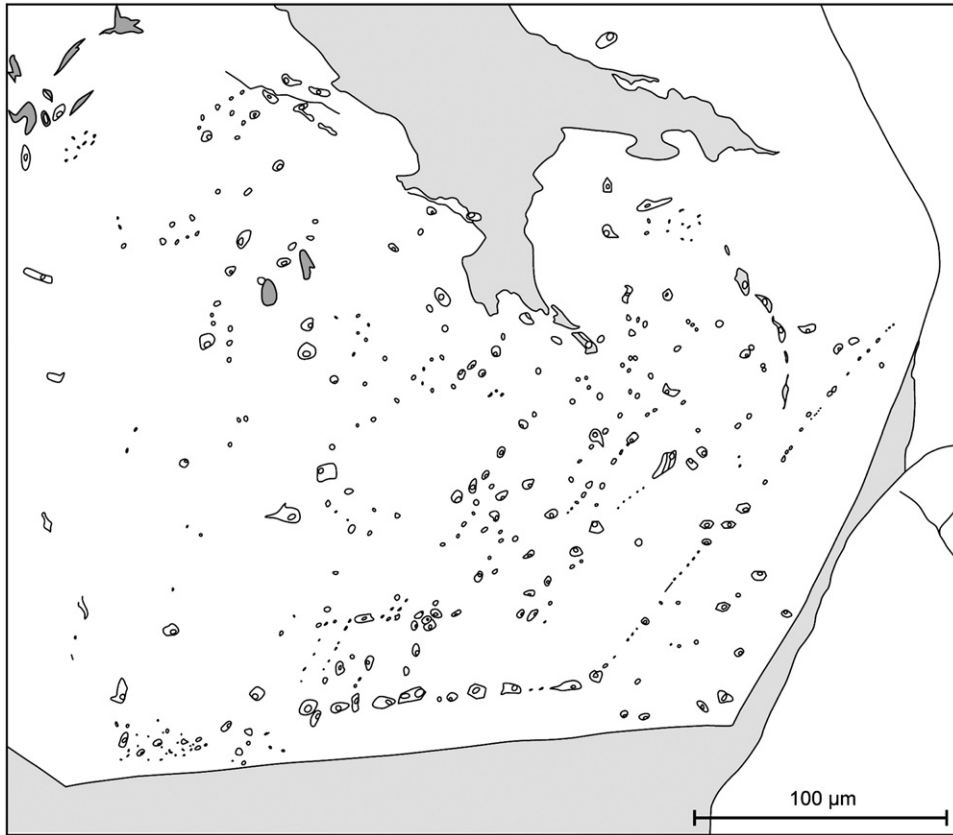


Fig. 5. Inclusions in sample SV01-23, grain 2. Part of the inclusions is distinctly aligned along the growth zones of the quartz crystal that hosts them.

4.2. Spatial distribution of the inclusions

The hypothesis that the analysed inclusions are primary, and therefore contain the oldest fluids, is supported by a number of arguments based on the distribution of the inclusions within the quartz grains: (a.) Some grains show a number of inclusions that are distinctly aligned along the growth zones of the quartz (e.g. Fig. 5, SV01-23 grain 2). (b.) The analysed inclusions are generally irregularly distributed throughout the grain, without any obvious planar alignment. (c.) The crystals are mostly undeformed. Aqueous inclusions are most abundant, but the relative amount of carbonic (type C) inclusions is variable in each grain. This indicates that each of the grain has its own population, related to its internal structure, formed during the growth of the host crystal.

In sample SV01-24b, the growth zones are characterised by slight colour differences within the quartz grains (Fig. 6a). The shape and amount of inclusions do not seem to be related to these zones. The micro-thermometric characteristics (see below) of the inclusions are occasionally, and only slightly, correlated with the growth zones.

In addition to the large clustered inclusions, smaller inclusions occur aligned along intra-grain trails perpendicular to the growth zones. Combined with the bimodal distribution of the inclusion sizes, this could indicate that post-trapping transposition took place. However, inclusions along the intra-grain trails have the same micro-thermometric characteristics (see below) as the rest of the inclusions. Hence, they are pseudo-secondary inclusions, which were formed during growth of the host crystal (cf. Roedder, 1984).

A strong bimodal size distribution among the aqueous inclusions is also observed in sample SV01-23, grain 1 (Fig. 7). The smaller inclusions in this grain may represent transposed inclusions, which resulted from post-trapping changes. Since the smaller inclusions have roughly the same liquid/vapour ratio as the larger inclusions, measurements on the larger inclusions are thought to be representative of the entire inclusion population. In the same grain, some elongated inclusions are present near the grain boundaries (e.g. lower left corner, Fig. 7). However, in the bulk of the

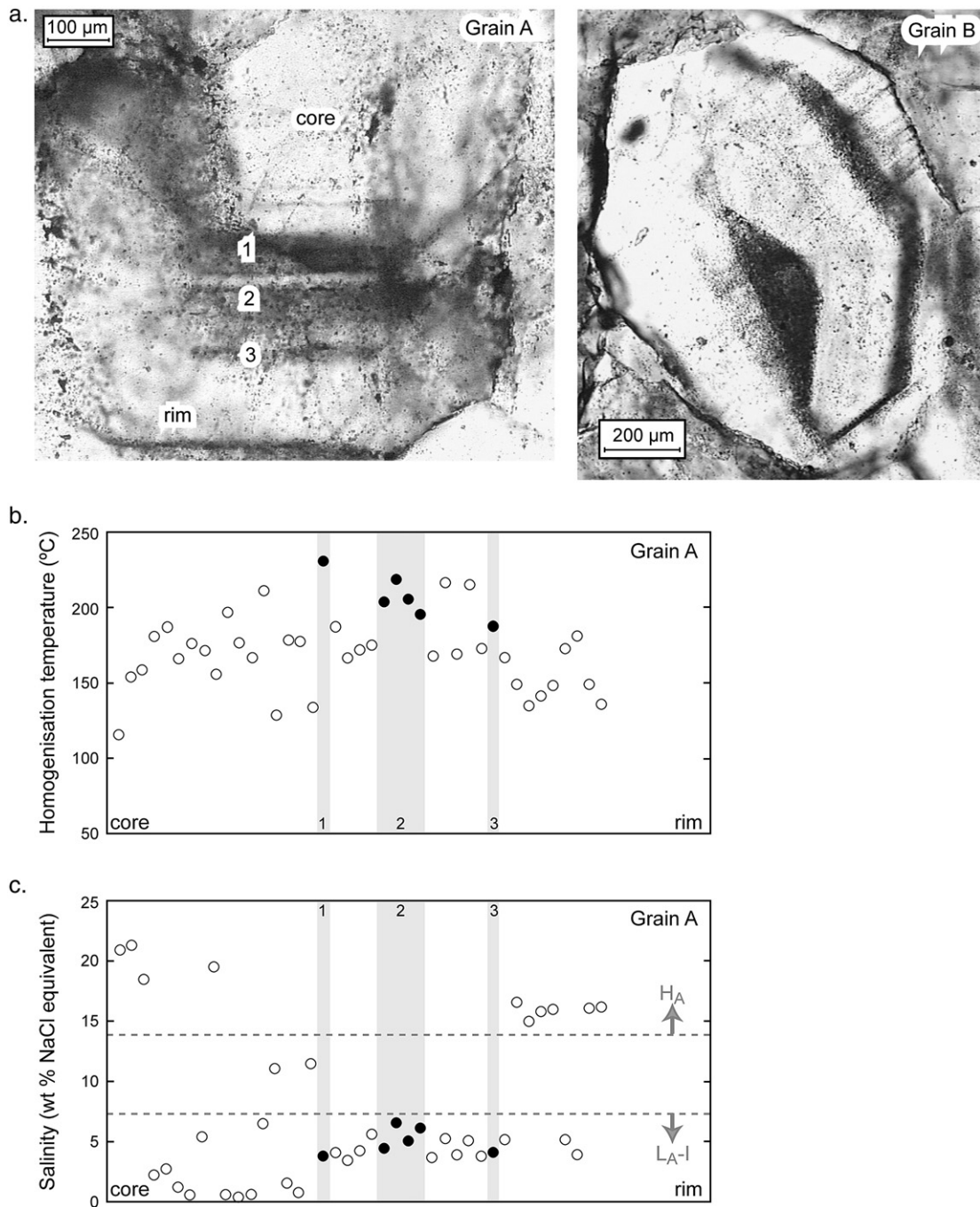


Fig. 6. Sample SV01-24b. a. Microphotographs of grains A and B, showing growth zones in quartz. b. Relationship between growth zoning and homogenisation temperature in grain A. c. Relationship between growth zoning and salinity in grain A. Numbered dark growth zones in Fig. a correspond to grey shaded, numbered bands in Figs. b and c.

grain the inclusions are spherical to elliptical. This may indicate local post-trapping modification, however, these changes appear to have remained minor, as indicated by the microthermometric data.

4.3. Microthermometric data

Based on microthermometric measurements, the aqueous liquid+vapour inclusions of the first category

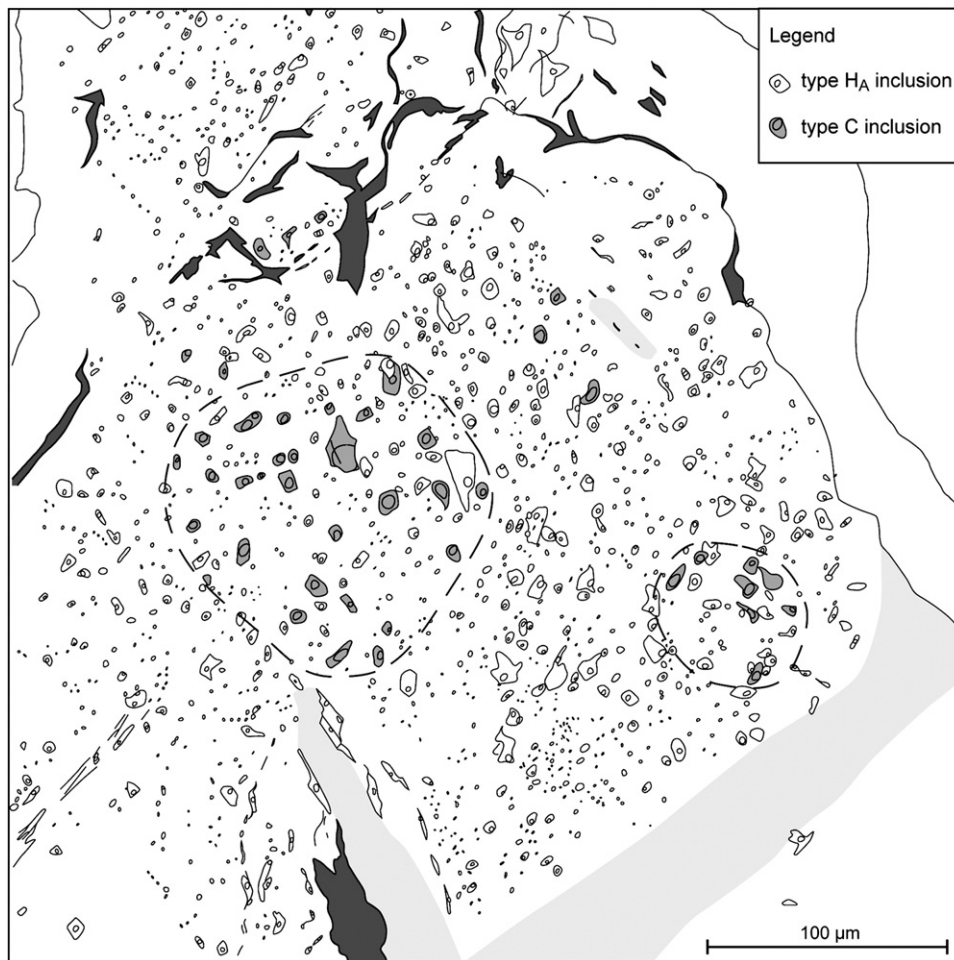


Fig. 7. Inclusions in sample SV01-23, grain 1. High-salinity aqueous inclusions (type H_A) are dominant in this grain. Low-salinity mixed H_2O – CO_2 inclusions (type C, grey shaded) occur as discrete domains within the group of high-salinity aqueous inclusions. Domains are indicated with dashed lines.

were subdivided into three types; high-salinity (type H_A), intermediate-salinity (type M_A), low-salinity (type L_A) inclusions. The microthermometric results for the three types of aqueous inclusions are summarised in Table 1 and Fig. 8. The CO_2 – H_2O (type C) inclusions were not subdivided. A summary of the microthermometric characteristics of this type of inclusions is given in Fig. 3b.

4.3.1. Aqueous inclusions

4.3.1.1. *Type H_A (high salinity)*. The final melting temperatures of ice, $T_{m(ice)}$, in type H_A inclusions range from -16.2 to -8.8 °C, which corresponds to salinities of 19.6–12.6 wt.% NaCl equivalent (salinities calculated from the freezing point depressions given by Bodnar and Vityk,

Table 1
Summary of microthermometric data for the four groups of aqueous inclusions

| Type | T_m range (°C) | T_m average (°C) | NaCl range (%) | NaCl average (%) | Th* range (°C) | Th* average (°C) |
|------------|------------------|--------------------|----------------|------------------|----------------|------------------|
| H_A | –18.8 to –8.4 | –12.2 | 21.5 to 12.2 | 16.0 | 115.7 to 199.8 | 153.9 |
| M_A | –8.3 to –4.1 | –6.7 | 12.1 to 6.6 | 10.1 | 96.0 to 160.0 | 130.0 |
| L_{A-II} | –4.4 to –2.2 | –3.2 | 7.0 to 3.7 | 5.3 | 97.8 to 116.5 | 106.1 |
| L_{A-I} | –4.2 to –1.4 | –2.9 | 6.7 to 2.4 | 4.7 | 140.9 to 216.1 | 182.2 |

T_m = final melting temperature, T_h = homogenisation temperature, NaCl = % NaCl equivalent.

*Always liquid homogenisation.

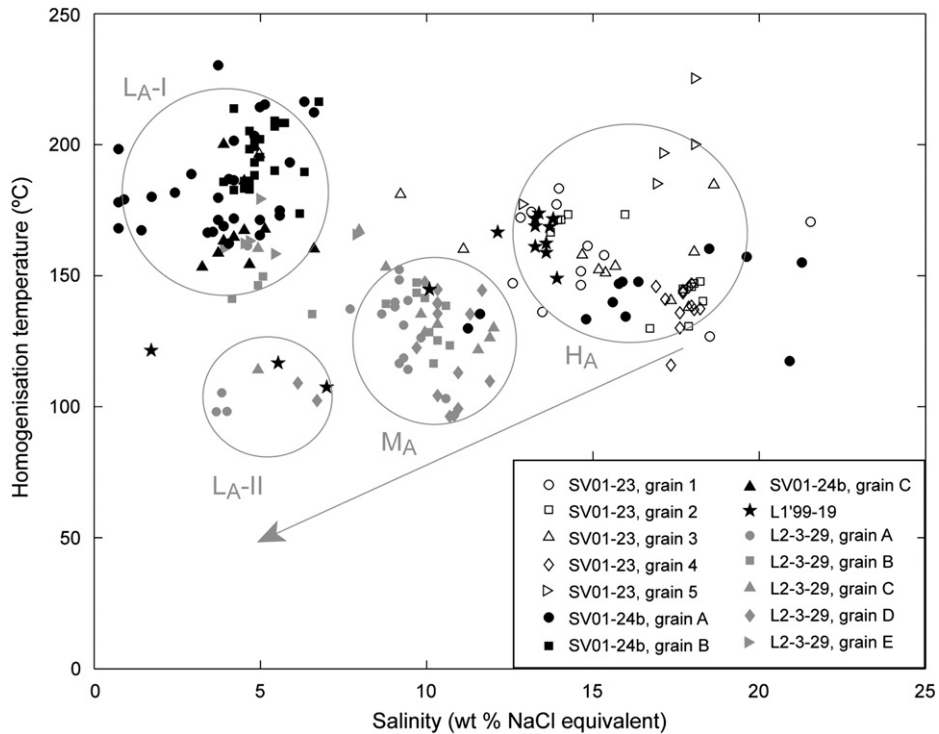


Fig. 8. Homogenisation temperature against salinity for all analysed two-phase aqueous inclusions from the Buck Ridge Chert. Arrow indicates trend from H_A to M_A to L_{A-II} . CO_2 -bearing inclusions are not shown in this figure.

1994). The homogenisation temperatures (to liquid) are in the range of 116–200 °C.

4.3.1.2. Type M_A (intermediate salinity). The $T_{m(lce)}$ values of type M_A inclusions are clearly higher than that of type H_A inclusions, and range between -8.3 and -4.9 °C. This corresponds to salinities between 12.1 and 7.7 wt.% NaCl equivalent. Homogenisation temperatures are slightly lower than those of type H_A inclusions, between 96 and 152 °C.

4.3.1.3. Type L_A (low salinity). Type L_A inclusions have relatively high $T_{m(lce)}$ values (-4.4 to -0.4 °C) and corresponding low salinities, between 7.0 and 0.7 wt.% NaCl equivalent. Most analyses combine to form a group with relatively high homogenisation temperatures, between 141 and 216 °C (type L_{A-I}). Nine analyses show significantly lower homogenisation temperatures (T_h), ranging between 98 and 117 °C, suggesting the existence of a second type of low-salinity inclusion (type L_{A-II}).

4.3.2. CO_2 -bearing inclusions (type C)

The average $T_{m(CO_2)}$ in the carbonic inclusions is around -57.6 °C, about one degree below the melting temperature

of the standard, indicating the presence of almost pure CO_2 . No ice melting could be seen. However, in several inclusions CO_2 -clathrate was observed to dissociate between 8.3 and 10 °C. CO_2 homogenisation temperatures (to liquid) vary between 9 and 22 °C, with a peak around 17 °C (Fig. 9). Total homogenisation temperatures could not be measured, as inclusions started to decrepitate around 225 °C, prior to homogenisation. However, shrinkage of

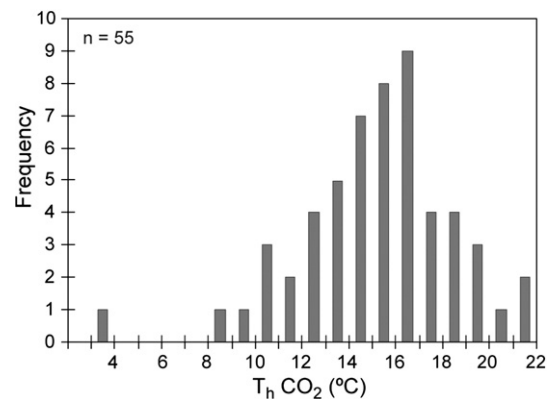


Fig. 9. Frequency histogram of homogenisation temperatures for type C inclusions (T_{hCO_2}) in sample SV01-23.

the carbonic bubble upon heating shows that homogenisation would occur to the liquid phase.

From these data and the relative volumes ($\text{CO}_2/\text{H}_2\text{O}$) at room temperature (Fig. 4), fluid molar volumes and composition can be estimated, either graphically (Diamond, 2001), or analytically, by calculating the mole number of the different species (Touret, 1977; Ramboz et al., 1982; Ramboz, pers.com.). Taking as limits $T_{\text{hCO}_2}=+10\text{ }^\circ\text{C}$, $V_{\text{CO}_2}/V_{\text{total}}=0.60$ and $T_{\text{hCO}_2}=+20\text{ }^\circ\text{C}$, $V_{\text{CO}_2}/V_{\text{total}}=0.35$, respectively, results from both methods differ only slightly: The graphic technique indicates a CO_2 mole fraction (X_{CO_2}) of 0.18–0.35 and a total molar volume (V_{tot}) of 25–31 $\text{cm}^3\text{ mol}^{-1}$, whereas the analytical approach (for V_{CO_2} relative volume of 0.55 and 0.30) gives an X_{CO_2} of 0.14–0.32, and a V_{tot} of 23.3–28.3 $\text{cm}^3\text{ mol}^{-1}$, corresponding to densities of 0.932 and 0.924 g/cm^3 , respectively (C. Ramboz, pers.com.). Note that, because of the large difference in molar volumes and smaller difference in density be-

tween CO_2 and H_2O , type C inclusions are more water-rich than the visual observation of relative volumes at room temperature would suggest: 50 vol.% CO_2 corresponds only to about 20 mol% CO_2 . In addition, the graphic method indicates that, if the inclusions had not decrepitated, total homogenisation would have occurred to the liquid phase between 260 and 273 $^\circ\text{C}$, at an internal pressure of more than 2 kb.

5. Interpretation

5.1. Spatial distribution of the aqueous inclusions

The summary diagram of all T_{h} and salinity data for the aqueous inclusions (Fig. 8) shows a relatively clear trend from H_A to M_A to L_{A-II} . From H_A to L_{A-II} , the salinity decreases from about 20 to 5 wt.% NaCl equivalent, while the homogenisation temperature decreases from 190 to 100 $^\circ\text{C}$. The relatively high temperature,

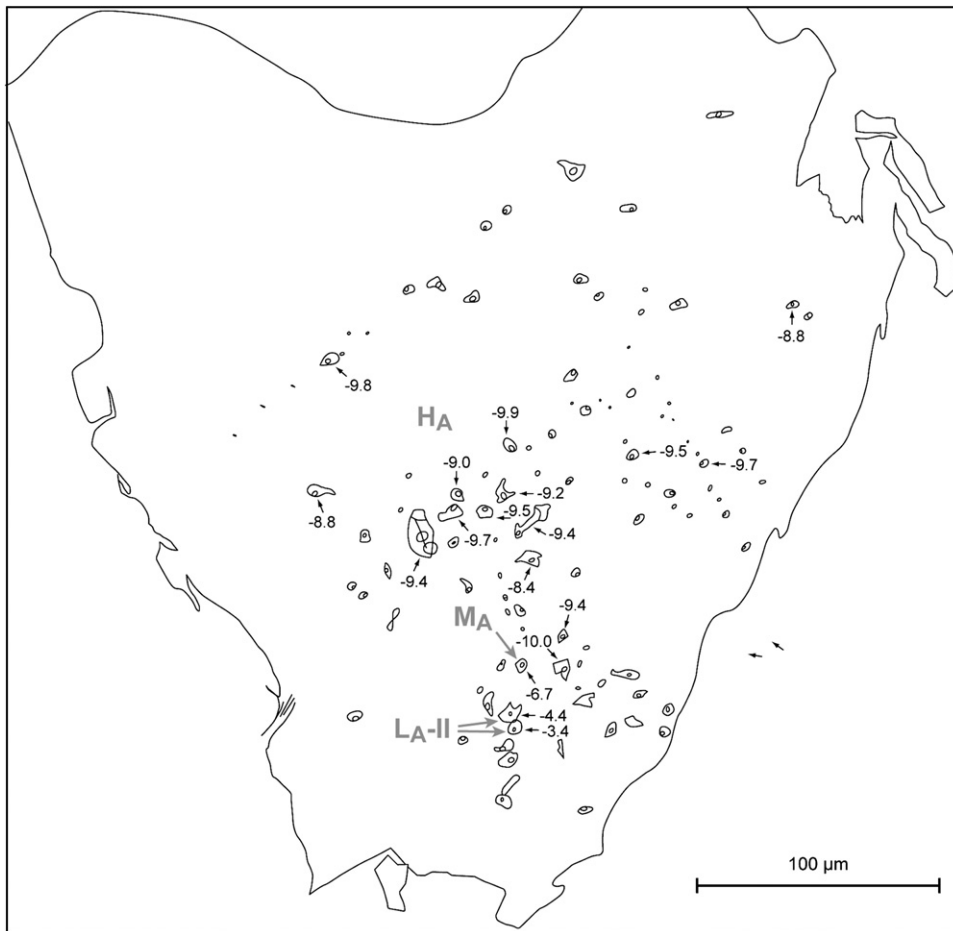


Fig. 10. Inclusions in sample SV99-L1-19. Within this quartz grain, there seems to be a very slight trend from type H_A to type M_A through to type L_{A-II} inclusion groups from the core to the margin of the grain. Final melting temperatures (in $^\circ\text{C}$) of measured inclusions are indicated.

low-salinity fluid L_{A-I} is apparently independent of this trend. The spatial distribution of the different inclusion types in the quartz grains does not show a clear relationship between the different aqueous groups. Moreover, in grains with distinct growth zones, no systematic relationship was found between inclusion characteristics and the successive growth zones. Nevertheless, the inclusion distribution is not completely random. Some grains show domains, of approximately hundred micrometer in size, in which one type is dominant or exclusive, such as in SV99-L1-19, where type H_A inclusions are dominant in the central part of the grain (Fig. 10). The inclusions in this grain display a very slight trend from L_{A-II} to M_A through to H_A groups from the margin to the core of the grain (see also discussion of T_h vs. salinity diagram below). In SV01-24b, grain A, two well defined H_A and L_{A-I} groups show the same homogenisation temperature (Fig. 6b). L_{A-I} type inclusions occur throughout the sample, whereas H_A type inclusions are restricted to the core and the outer margin of the grain (Fig. 6c).

5.2. Immiscibility between high-salinity aqueous (type H_A) and CO_2 -bearing (type C) inclusions

The relatively constant V_{CO_2}/V_{total} ratio of type C inclusions (Fig. 4), the monopeak histogram of the CO_2 homogenisation temperature (Fig. 9), and corresponding relatively constant CO_2 and total molar volumes (see above), indicate that the fluid was a homogeneous mixture of H_2O and CO_2 at the time of trapping. Type C inclusions are homogeneous, and occur in discrete domains of $\sim 100 \mu m$ within the grain, surrounded by also homogeneous, more regularly dispersed type H_A inclusions (Fig. 7). The two fluids were coeval: virtually all inclusions are primary (only exceptionally pseudo-secondary) with respect to the host crystal, and the small size of the domains in which they occur indicates that they were trapped during a short period of crystal growth. In short, type C and type H_A fluids meet the basic criteria of fluid immiscibility, as defined in the fluid inclusion literature (e.g. Roedder, 1984). The immiscibility may have resulted either from unmixing of an initially homogeneous $CO_2-H_2O-NaCl$ fluid phase, or from mechanical mixing of fluids issued from different sources. Despite the problems that it creates for pressure–temperature interpretation (see below), the first hypothesis is preferred:

1) If mechanical mixing between CO_2 -rich and NaCl-rich aqueous fluids had occurred, a continuous variation (mixing line) between the CO_2 - and NaCl-

bearing end members would be expected. Such a mixing line between the two fluids is not observed here. Occasionally, mixing of both types may have occurred, leading to salinity fluctuations in type H_A inclusions and to sporadic precipitation of calcite crystals (resulting from the reaction between the CO_2 -component of the type C fluid and the dissolved ions in the highly saline type H_A fluid). However, on the whole, salinities of aqueous components in type C and type H_A fluids differ significantly within individual grains. For instance, in grain 1 of sample SV01-23, low-salinity mixed H_2O-CO_2 inclusions (type C) and high-salinity aqueous inclusions (type H_A) occur together (Fig. 7). Mixing may have occurred within the different purely aqueous fluid types H_A , M_A and L_A (Fig. 8, see above). However, this mixing occurs at a larger scale than a single grain, more distal in the hydrothermal system.

2) Many studies on quartz crystals containing fluids of different origins (primarily of magmatic versus

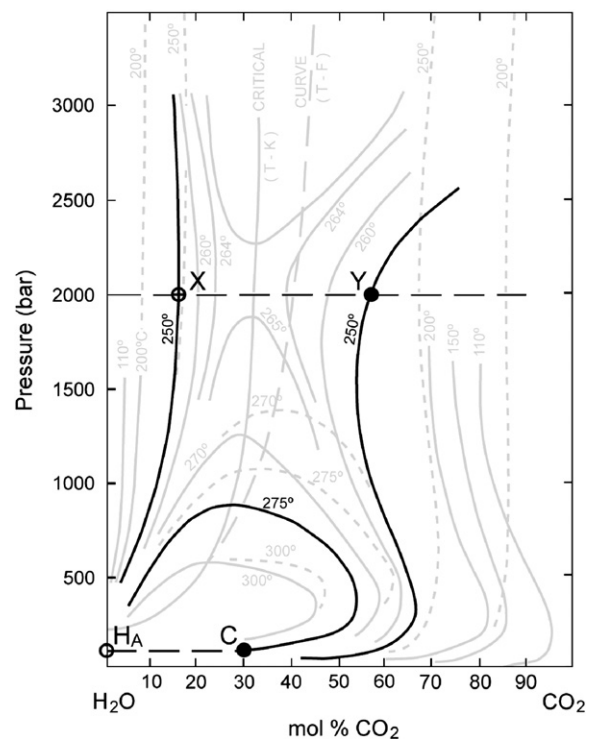


Fig. 11. Pressure-composition section for the H_2O-CO_2 system (Fyfe et al., 1978). The immiscibility surface is defined by isotherms ($^{\circ}C$). Solid lines: Takenouchi and Kennedy (1964), dashed lines: Töðheide and Franck (1963). At $P-T$ conditions of ~ 2000 bars and $250^{\circ}C$, two coexisting fluids such as X and Y, cannot have H_A and C compositions: fluid Y is much richer in CO_2 than fluid C. Only at low pressures (~ 100 bars) fluids with C and H_A compositions can coexist along the immiscibility surface.

meteoric origin; Sauniac and Touret, 1983; Touret and Dietvorst, 1983 and unpublished studies by Touret) have shown that, in these cases, the different fluid types are not strictly coeval. They occurred either in different growth zones within the quartz host or, more commonly, along different systems of healed micro-fractures (i.e. as secondary or pseudo-secondary inclusions). All inclusions measured in the present study are primary with respect to their mineral host, and the different inclusion types are unrelated to different growth zones.

5.3. Pressure–temperature conditions of fluid trapping

Fluid immiscibility as observed for type C and H_A inclusions, poses a major problem for the determination of *P–T* conditions of fluid trapping. Inclusions showing a homogeneous H₂O–CO₂ fluid content (type C) are normally considered to have formed above or along the immiscibility surface (boiling) of the fluid system. In that case, total homogenisation would occur at ~270 °C (260–273 °C, Section 4.3.2), for an internal pressure of more than 2 kb. These estimates, in line with decrepitation at about 225 °C, which should occur at a pressure of ~1.5 kb (Naumov and Malinin, 1968), represent minimum trapping conditions for this fluid type.

However, such conditions are at odds with the regional geological context, notably with the shallow environment of deposition of the Buck Ridge Chert sediments, the evidence for (almost) contemporaneous hydrothermal activity in the sediments and the very low metamorphic grade. A pressure of ~2 kb would correspond to a depth of 6–8 km, many times more than expected from the near-surface depth of deposition indicated by field observations. This apparent contradiction could be explained if hydrothermal fluids were pressurised, at a pressure largely in excess of regional lithostatic pressure. It would imply that fluids were directly issued from the magmatic geothermal source, along a network of interconnected channels, for which a trapping pressure of the order of 2 kb is not unreasonable. Examples of regional fluid overpressure are also known from different environments, notably Alpine veins. For many veins, independent of the metamorphic grade, pressure at the initiation of the fracture may exceed the regional pressure by several kilobars, then drops markedly at vein opening, before slowly rising again during subsequent vein filling (e.g. Mullis et al., 1994).

In the present case, however, such interpretations are difficult to reconcile with the field observations.

Hydraulic fracturing indeed exists in the Buck Ridge Chert (e.g. sample SV01-24b), but only in a weak form, not showing the explosive character that would undoubtedly be caused by a fluid overpressure of several kilobars. Moreover, unmixing at a relatively high pressure raises another major problem, related to the unmixing characteristics of mixed aqueous–gaseous systems (C. Ramboz, pers. com.). Above a few hundred bars, isotherms of the H₂O–CO₂ immiscibility surface, which define the immiscibility field in the *P–T–V* space, are roughly parallel to the pressure axis (Fig. 11). Hence, at these pressures, a H₂O-rich fluid such as H_A can only coexist with an extremely CO₂-rich fluid (almost pure CO₂ if H_A is CO₂-free).

At a lower pressure, the situation changes drastically. Below about 1 kb, isotherms on the CO₂ side (275 to 300 °C), show a maximum CO₂ content of 40 to 60% at pressures slightly below 500 bars, before turning sharply towards the H₂O-rich pole at lower pressure (Fig. 11). Experimental data on this system, obtained by Tödheide and Franck (1963) and Takenouchi and Kennedy (1964), differ substantially from each other, but the trends of the isotherms are the same. For conditions that roughly correspond to type C-fluid of this study, i.e. $T_{h(\text{total})}=275$ °C and $X_{\text{CO}_2}=0.3$, Takenouchi and Kennedy's data give a pressure of about 100 bars (extrapolation of Tödheide and Franck's data gives virtually the same pressure; Fig. 11). The addition of an extra component (NaCl) to the H₂O–CO₂ mixture enlarges the immiscibility field, but it does not change the topology of the system. Therefore, the overall conclusion remains the same: Fluid unmixing of H_A and C must have occurred at relatively low pressure, lower than ~100 bars. This conclusion is in line with the geological context, as well as with the composition of the coexisting fluids. However, it does not comply with the homogeneous character of the type C fluids. A possible explanation for this would be that type C fluids were exsolved within the immiscibility field of the H₂O–CO₂ system, but we recognise that such a hypothesis poses a number of additional problems. At this point, it remains an unsolved problem how exactly type C fluids could fit in the regional context.

5.4. Fluid origin

Field relationships indicate that the quartz hosting the fluid inclusions originated from hydrothermal systems that were active contemporaneously with or immediately after deposition of the Buck Ridge volcano-sedimentary complex. Both microthermometric and visual characteristics of the inclusions point to a primary

origin of the inclusions, with only minor post-trapping changes. Therefore, the fluid inclusions are interpreted to have been unaffected by regional (low-grade) metamorphism of the area.

The salinities of type H_A and M_A inclusions are too low to represent dissolution of evaporites, but they are significantly higher than both the modern-day seawater salinity and the ~ 3.2 Ga seawater salinity interpreted by De Ronde et al. (1994). This could either be due to magmatic influence, or due to a highly saline seawater component in the fluid. The presence of CO_2 suggests that there is at least some magmatic component in the hydrothermal fluid. Further analysis of the fluids is necessary to determine whether part of the fluids is indeed of seawater origin (cf. De Ronde et al., 1997a). The trapping temperature of the inclusions is in the range of modern-day hydrothermal fluids. A fluid inclusion study of the active Los Azufres geothermal system (related to Los Azufres caldera, Mexico) yielded homogenisation temperatures of ~ 200 – 330 °C (Catherineau et al., 1989), and venting temperatures in mid-ocean ridge systems are ~ 180 – 400 °C (e.g. Spooner and Fyfe, 1973; Seyfried et al., 1999).

The trend from H_A to M_A to L_{A-II} in Fig. 10 may represent mixing of a high-salinity fluid with a low-salinity fluid at decreasing temperature. The relatively high T_h , low-salinity fluid (L_{A-I}) behaves in an apparently independent manner compared to this trend. One explanation is that L_{A-I} originated from the aqueous component of the C fluid. Pure CO_2 either escaped to a more superficial level, or was trapped in carbonates outside of the domain where L_{A-I} inclusions were formed.

5.5. Comparison with other Archaean hydrothermal systems

Fluid inclusion studies on roughly similar-aged hydrothermal systems were previously carried out in another, slightly younger, low-grade metamorphic part of the Barberton Greenstone Belt (South Africa), in the low-grade metamorphic North Pole area in the Pilbara (Australia), and in the medium to high-grade metamorphic Isua Greenstone Belt (Greenland).

De Ronde et al. (1994, 1997a) studied fluid inclusions from mid Archaean ironstone pods in the Barberton Greenstone Belt, which were interpreted as hydrothermal discharge zones of the seafloor. From fluid inclusion data they interpreted that ~ 3.2 Ga vent fluids had chemical and isotopic signatures similar to those of modern vents. The seawater salinity and chemistry in the mid-Archaean were also rather similar to those of today,

except for the halide ratios and higher concentrations of Ca, Sr and NH_4 .

Kitajima et al. (2001a,b) studied inclusions in barite and quartz veins below the ~ 3.49 Ga old North Pole chert–barite unit (Pilbara). They found a hydrothermal fluid that they interpreted to have boiled or phase-separated at about 150 °C and 1000 m below the seafloor. They concluded that, because of mixing of this fluid with cold seawater during its ascent below the seafloor, the vent fluids were relatively cold (<150 °C). However, Kitajima et al. (2001a,b) interpreted the chert–barite unit and the contemporaneous vein systems as having developed in a mid-ocean ridge setting, whereas there is a general agreement that the North Pole chert–barite unit was deposited in shallow water (e.g. Dunlop et al., 1978; Barley et al., 1979; Dunlop and Buick, 1981; Nijman et al., 1998).

Sea-floor hydrothermal systems appear to have remained relatively constant throughout the Earth's history, as early to mid-Archaean environments can be interpreted in terms of present-day settings. This conclusion can possibly even be extended to the oldest known example of a seafloor hydrothermal system, based on the preservation of pre-metamorphic fluids in >3.75 Ga old altered pillow basalts of the Isua Greenstone Belt, Greenland (Appel et al., 2001). Inclusions from quartz vesicles in these pillow basalts contain remnants of two independent fluid/mineral systems; either gases (CH_4 or CO_2 , both pure in separate inclusions) or highly saline aqueous fluids (~ 25 wt.% NaCl equivalent). The latter bear a strong resemblance to modern sea floor hydrothermal fluids and were interpreted to be responsible for the alteration of the pillow fragments. The interpretation of these inclusions as being original, i.e. >3.75 Ga old, is controversial however, since the entire surrounding rock sequence at that location has experienced medium to high-grade amphibolite facies metamorphism (e.g. Rosing and Frei, 2004). Touret (2003) interpreted the higher salinities and the more reduced character of the gaseous component of the inclusion in the Isua Greenstone Belt as an indication of higher seawater salinities around 3.8 Ga, and deposition in a deep-water, mid-ocean ridge type environment. However, more recent investigations (Heijlen et al., 2005, 2006) suggest that these conclusions must be re-evaluated as far as gasses are concerned. The occurrence of methane, in particular, is related to CO_2 reduction during post-metamorphic quartz deformation and annealing. The earliest fluids would correspond to an immiscible mixture of brines and CO_2 , in that respect comparable to what has been described in the present work.

6. Conclusions

Hydrothermally deposited quartz in the Buck Ridge volcano-sedimentary complex (Barberton Greenstone Belt, South Africa) contains coeval two-phase aqueous inclusions (with variable salinities) and mixed H₂O–CO₂ inclusions. These fluids are interpreted to be at least partly of magmatic hydrothermal origin. High-salinity aqueous inclusions and low-salinity mixed H₂O–CO₂ inclusions show unmixing, which must have occurred at a relatively low pressure of ~100 bars. This conclusion is in line with the geological context, but contrary to the first impression given by the homogeneous character of the mixed H₂O–CO₂ inclusions. Unmixing between the high-salinity aqueous and mixed H₂O–CO₂ fluids was probably associated with the opening of the hydrothermal veins. Low-salinity aqueous fluids may have resulted from mixing with lower temperature fluids, probably issued from the H₂O component of the mixed H₂O–CO₂ fluid.

The similarities of the aqueous fluids compared to those of present day hydrothermal systems, and the absence of reduced gases in inclusions from the Buck Ridge Chert, strengthen the conclusion from field observations that the BR-vsc hydrothermal system operated in a shallow water, near-surface environment.

Acknowledgements

STdV thanks Cornel de Ronde for initially advising her on the practical aspects of fluid inclusion studies during her visit to the Institute of Geological and Nuclear Sciences (New Zealand) in 2000. We are grateful for the help of Eduardo Campos Sepúlveda and Bin Fu during microthermometric measurements in the lab at the Free University of Amsterdam. Technical support at the Free University was provided by Wim Lustenhouwer. We thank Wout Nijman, Cornel de Ronde, Poppe de Boer, Maarten de Wit, Maria-Luce Frezzotti, Fons van den Kerkhof and especially Clairette Ramboz for discussions and comments on earlier versions of the manuscript, which helped to improve this article. Constructive reviews by Larry W. Diamond and Ilka Kleinhanns are gratefully acknowledged. Fieldwork for this study was supported by the Foundation Dr. Schürmannfonds, grants 1999/14 and 2001/14.

References

- Appel, P.W.U., Rollinson, H.R., Touret, J.L.R., 2001. Remnants of an Early Archaean (>3.75 Ga) sea-floor, hydrothermal system in the Isua Greenstone Belt. *Precambrian Res.* 112, 27–49.
- Barley, M.E., Dunlop, J.S.R., Glover, J.E., Groves, D.I., 1979. Sedimentary evidence for an Archaean shallow-water volcanic-sedimentary facies, Eastern Pilbara Block, Western Australia. *Earth Planet. Sci. Lett.* 43, 74–84.
- Bodnar, R.J., Vityk, M.O., 1994. Interpretation of microthermometric data for H₂O–NaCl fluid inclusions. In: De Vivo, B., Frezzotti, M.L. (Eds.), *Fluid Inclusions in Minerals: Methods and Applications*. Virginia Polytechnic Institute and State University, pp. 117–130.
- Cathelineau, M., Izquierdo, G., Nieva, D., 1989. Thermobarometry of hydrothermal alteration in the Los Azufres geothermal system (Michoacan, Mexico): significance of fluid-inclusion data. *Chem. Geol.* 76, 229–238.
- De Ronde, C.E.J., De Wit, M.J., Spooner, E.T.C., 1994. Early Archaean (>3.2 Ga) Fe-oxide-rich, hydrothermal discharge vents in the Barberton Greenstone Belt, South Africa. *Geol. Soc. Amer. Bull.* 106, 86–104.
- De Ronde, C.E.J., Channer, D.M., De, R., Faure, K., Bray, C.J., Spooner, E.T.C., 1997a. Fluid chemistry of Archaean seafloor hydrothermal vents: implications for the composition of circa 3.2 Ga seawater. *Geochim. Cosmochim. Acta* 61, 4025–4042.
- De Ronde, C.E.J., Channer, D.M., De, R., Spooner, E.T.C., 1997b. Archaean fluids. In: De Wit, M.J., Ashwal, L.D. (Eds.), *Greenstone Belts*. Oxford Monogr. Geol. Geophys. Clarendon Press, Oxford, pp. 309–335.
- De Vries, S.T., 2004. Early Archaean sedimentary basins: depositional environment and hydrothermal systems. Examples from the Barberton and Coppin Gap Greenstone Belts. *Geologica Ultraiectina*, vol. 244, p. 160.
- De Vries, S.T., Nijman, W., De Boer, P.L., in preparation. Early Archaean sedimentary rocks of the Buck Ridge (South Africa) and Kittys Gap (Western Australia) volcano-sedimentary complexes. To be submitted to *Sedimentology*.
- De Vries, S.T., Nijman, W., Armstrong, R.A., 2006. Growth-fault structure and stratigraphic architecture of the Buck Ridge volcano-sedimentary complex, upper Hooggenoeg Formation, Barberton Greenstone Belt, South Africa; a framework for Archaean basin studies. *Precambrian Res.* 149, 77–98.
- De Wit, M.J., Ashwal, L.D., 1997. *Greenstone Belts*. Oxford Monographs on Geology and Geophysics, vol. 35. Clarendon Press, Oxford, p. 809.
- Diamond, L.W., 2001. Review of the systematics of CO₂–H₂O fluid inclusions. *Lithos* 55, 69–99.
- Dunlop, J.S.R., Buick, R., 1981. Archaean epiclastic sediments derived from mafic volcanics, North Pole, Pilbara Block, Western Australia. *Spec. Publ. - Geol. Soc. Aust.* 7, 225–233.
- Dunlop, J.S.R., Muir, M.D., Milne, V.A., Groves, D.I., 1978. A new microfossil assemblage from the Archaean of Western Australia. *Nature* 274, 676–678.
- Fyfe, W.S., Price, N.J., Thompson, A.B., 1978. Fluids in the Earth's crust. *Dev. Geochemistry*, vol. 1. Elsevier, Amsterdam. 381 pp.
- Heijlen, W., Appel, P.W.U., Frezzotti, M.L., Touret, J.L.R., 2005. Fluids in inclusions from well-preserved pillow basalt breccia of the ca 3.75 Ga Isua Greenstone Belt: sea-floor hydrothermal or metamorphic origin. *ECROFI XVIII, Siena, Abstr. Vol.*
- Heijlen, W., Appel, P.W.U., Frezzotti, M.L., Horswell, A., Touret, J.L.R., 2006. Metamorphic fluid flow in the northeastern part of the 3.8–3.7 Ga Isua Greenstone Belt (SW Greenland): a re-evaluation of fluid inclusion evidence for early Archaean sea-floor hydrothermal systems. *Geol. Cosmochim. Acta.* 70, 3075–3095.
- Kisch, H.J., Nijman, W., 2004. Metamorphic grade from K-micas in the metasediments of the Pilbara and Barberton Greenstone Belts.

- In: Reimold, W.U., Hofmann, A. (Eds.), Abstract Volume, Field Forum on Processes on the Early Earth, Kaapvaal Craton, South Africa, pp. 47–48. 4–9 July.
- Kitajima, K., Kabashima, T., Ueno, Y., Terabayashi, M., Maruyama, S., 2001a. Archaean seafloor hydrothermal system in the North Pole of the Pilbara Craton, Western Australia. In: Cassidy, K.F., Dunphy, J.M., Van Kranendonk, M.J. (Eds.), 4th International Archaean Symposium. AGSO — Geoscience Australia, Perth, pp. 51–53.
- Kitajima, K., Maruyama, S., Utsunomiya, S., Liou, J.G., 2001b. Seafloor hydrothermal alteration at an Archaean mid-ocean ridge. *J. Metamorph. Geol.* 19, 583–599.
- Lowe, D.R., Byerly, G.R., 1999. Stratigraphy of the west-central part of the Barberton Greenstone Belt, South Africa. In: Lowe, D.R., Byerly, G.R. (Eds.), *Geologic Evolution of the Barberton Greenstone Belt, South Africa*. *Geol. Soc. Am. Spec. Paper*, vol. 329, pp. 1–36.
- Mercolli, I., 1979. Le inclusioni fluide nei noduli di quarzo dei marmi dolomitici della regione del Campolungo (Ticino). PhD Thesis, ETH, Zurich, 138 pp.
- Mullis, J., Dubessy, J., Poty, B., O'Neil, J., 1994. Fluid regimes during late stages of a continental collision: physical, chemical, and stable isotope measurements of fluid inclusions in fissure quartz from a geotraverse through the Central Alps, Switzerland. *Geochim. Cosmochim. Acta* 58, 2239–2267.
- Naumov, V.B., Malinin, S.D., 1968. A new method for determining pressure by means of gas–liquid inclusions. *Geochem. Int.* 5, 382–391.
- Nijman, W., De Bruijne, C.H., Valkering, M.E., 1998. Growth fault control of Early Archaean cherts, barite mounds and chert–barite veins, North Pole Dome, Eastern Pilbara, Western Australia. *Precambrian Res.* 88, 25–52.
- Ramboz, C., Pichavant, M., Weisbrod, A., 1982. Fluid immiscibility in natural processes: use and misuse of fluid inclusion data. II: interpretation of fluid inclusion data in terms of immiscibility. *Chem. Geol.* 37, 29–48.
- Roedder, E., 1984. Fluid inclusions. *Rev. Miner.* 12, 644.
- Rosing, M.T., Frei, R., 2004. U-rich Archaean sea-floor sediments from Greenland — indications of >3700 Ma oxygenic photosynthesis. *Earth Planet. Sci. Lett.* 217, 237–244.
- Sauniac, S., Touret, J.L.R., 1983. Petrology and fluid inclusions of a quartz–kyanite segregation in the main thrust zone of the Himalayas. *Lithos* 16, 35–45.
- Seyfried, W.E.J., Ding, K., Berndt, M.E., Chen, X., 1999. Experimental and theoretical controls on the composition of mid-ocean ridge hydrothermal fluids. In: Barrie, C.T., Hannington, M.D. (Eds.), *Volcanic-Associated Sulfide Deposits: Processes and Examples in Modern and Ancient Settings*. *Rev. Econ. Geol.*, vol. 8, pp. 181–200.
- Spooner, E.T.C., Fyfe, W.S., 1973. Sub-sea-floor metamorphism, heat and mass transfer. *Contrib. Mineral. Petrol.* 42, 287–304.
- Takenouchi, S., Kennedy, G.C., 1964. The binary system H₂O–CO₂ at high temperatures and pressures. *Am. J. Sci.* 262, 1055–1074.
- Tödheide, K., Franck, E.U., 1963. Das Zweiphasengebiet und die kritische Kurve im System Kohlendioxid-Wasser bis zu Drucken von 3500 bar. *Z. Phys. Chem., Suppl.heft (N. F.)* 37, 387–401.
- Touret, J.L.R., 1977. The significance of fluid inclusions in metamorphic rocks. In: Fraser, D.G. (Ed.), *Thermodynamics in Geology*. D. Reidel Publishing Company, Dordrecht-Holland, pp. 203–227.
- Touret, J.L.R., 2003. Remnants of early Archaean hydrothermal methane and brines in pillow-breccia from the Isua Greenstone Belt, West Greenland. *Precambrian Res.* 126, 219–233.
- Touret, J.L.R., Dietvorst, P., 1983. Fluid inclusions in high grade anatectic metamorphites. *J. Geol. Soc. (Lond.)* 140, 635–649.